Journal of Power Sources 208 (2012) 415–420

Contents lists available at SciVerse ScienceDirect

Journal of Power Sources

journal homepage: www.elsevier.com/locate/jpowsour

Effect of oxygen partial pressure on the electrochemical impedance of $La_{0.8}Sr_{0.2}MnO_{3-\delta}/Zr_{0.92}Y_{0.08}O_2$ porous composite anodes in solid oxide electrolysis cell

Jing Wang*, Yong Zhang, Tongxiang Liang, Changsheng Deng**, Jingming Xu

Beijing Fine Ceramics Laboratory, State Key Laboratory of New Ceramics and Fine Processing, Institute of Nuclear and New Energy Technology, Tsinghua University, Beijing 100084, PR China

ARTICLE INFO

Article history:
Received 3 September 2011
Received in revised form 16 February 2012
Accepted 18 February 2012
Available online 25 February 2012

Keywords:
Solid oxide electrolysis cell
Porous composite anode
Oxygen partial pressure
Impedance spectroscopy

ABSTRACT

The electrochemical behavior of the $La_{0.8}Sr_{0.2}MnO_{3-\delta}/Zr_{0.92}Y_{0.08}O_2$ (LSM/YSZ) porous composite anodes in solid oxide electrolysis cell is investigated by impedance spectroscopy over an oxygen partial pressure (pO_2) range from 0 to 0.6×10^5 Pa. The differential analysis of impedance spectra (DIS) shows three separate arcs which correspond to three different electrode processes at high, intermediate and low frequencies, respectively. Three different electrode processes can be attributed to the migration of oxygen ions from the electrolyte to the triple-phase boundary, concentration impedance associated with dissociative desorption of O^{2-} along the LSM surface and diffusion of oxygen, respectively. Interestingly, under low pO_2 (≈0 Pa), the impedance arcs become clearly separated at different frequencies, especially for the anodes with higher porosity. Meanwhile, the results demonstrate that the electrode process associated with the low-frequency arc is strongly affected by pO_2. Furthermore, the porosity plays an important role in dissociative adsorption and diffusion of oxygen.

1. Introduction

Strontium-doped lanthanum manganite ($La_{1-x}Sr_xMnO_{3-\delta}$, LSM), which is known to have good electronic conductivity at high temperatures (650–1000 °C), is the most common electrode (anode) material for O^{2-} oxidation reaction in solid oxide electrolysis cells (SOEC) [1,2]. Pure LSM, however, with poor ionic conductivity hinders the improvement of electrode performance since electrochemical reactions only occur in a small area between the electrolyte ($Zr_{0.92}Y_{0.08}O_2$, YSZ) and the electrode (LSM). An effective way is to mix LSM and YSZ powders and fabricate composite anode, such that the electrochemical active area can be extended into certain depth of anode. Therefore, the interface of LSM and YSZ are critical in determining the electrochemical properties of the anode in SOEC.

Porosity has a significant effect on the electronic conductivity of the electrode, which has been attributed to changes in microstructure [3]. The electrical properties of porous materials are very complicated due to complex microstructure and huge internal surface area [4–6]. The porosity plays an important role in restricting the length of triple-phase boundary (TPB). Moreover, the length of TPB affects the polarization resistance (R_p) of LSM/YSZ electrode, and also changes the rate limiting step of O_2/O^{2-} reaction [7]. In fact, porous electrodes have numerous applications primarily because they promote intimate contact of the electrode material with the gaseous phase [8]. However, little is known about the mechanisms of charge and non-charge transfer in porous electrodes, especially in SOEC [9–13].

EIS (electrochemical impedance spectroscopy) of the LSM/YSZ anode is affected by not only the porosity of electrode, but also oxygen partial pressure (pO_2). pO_2 is related to oxygen nonstoichiometry of the LSM (δ in $La_{1-x}Sr_xMnO_{3-\delta}$) because the value of δ determines the electronic properties, such as the behavior of O^{2-} transfer, electronic conductivity and gas diffusion [14]. The EIS is a very sensitive technique to measure the R_p change with pO_2 [15]. Normally, the impedance spectra of the LSM/YSZ anode are composed of several overlapping arcs, which have been reported to consist of one to three depressed arcs [15–17]. However, different interpretations for intermediate and high-frequency arcs were reported [18]. The intermediate frequency arc was attributed to the surface diffusion of oxygen [19,20], dissociation and adsorption of oxygen on the LSM surface [21]. Van Heuveln et al. [22] reported that the high frequency arc is related to the charge transfer. While both Kim et al. [15] and Jiang et al. [19] claimed that the high-frequency arc is due to the O^{2-} transfer from TPB to the YSZ electrolyte.

* Corresponding author. Tel.: +86 10 51534440; fax: +86 10 89796022.
** Co-corresponding author.
E-mail addresses: wjing09@mails.tsinghua.edu.cn, wangjing99@gmail.com (J. Wang), changsheng@tsinghua.edu.cn (C. Deng).

0378-7753/$ – see front matter © 2012 Elsevier B.V. All rights reserved.
doi:10.1016/j.jpowsour.2012.02.061

To date, the influence of pO_2 on the anode performance has been quite limited. Thus, through the utilization of three kinds of porous anode, we have quantitatively measured the EIS as a function of pO_2. Here, we apply an approach based on differential analysis of impedance spectra (DIS) to compare the dependence of conductivity on pO_2 for porous LSM/YSZ composite anodes with different porosities.

2. Experimental

2.1. Material synthesis and sample preparation

The $La_{0.8}Sr_{0.2}MnO_{3-\delta}$ was synthesized by a solid-state reaction method. Firstly, the appropriate ratios of Lanthanum nitrate ($La(NO_3)_3{\cdot}6H_2O$, AR), strontium carbonate ($SrCO_3$, AR), manganous carbonate ($MnCO_3$, AR) were thoroughly mixed with alcohol using a ball mill. Subsequently, the alcohol was removed by heating the slurry at 120 °C in air for 12 h. Next, the resulting dry powder was then calcined at 1000 °C for 6 h in air. The obtained powders were ground, milled and finally sifted through 300 mesh. Finally the LSM powders were mixed with the YSZ (TZ-8Y, Tosoh Corporation, Japan) powders at a mass ratio of LSM/YSZ = 1.0 by ball milling for 10 h and then the composite powders were obtained.

Anode powders were prepared by mixing the desired quantities of composite powders and pore former. The starch was used as the pore former at the weight fractions of 5, 10, and 15 wt%, respectively. These anode powders were mixed in organic solvent and ball-milled for at least 6 h. Then, the anode slurries were obtained. The slurries were screen printed onto sintered YSZ discs with a thickness of 0.8 mm and a diameter of 19 mm. In order to obtain a desired electrode thickness of about 20 μm, four layers of the composite were deposited. Between each deposition, the layers were dried at 170 °C to evaporate the solvent. The samples were then sintered at 1200 °C for 2 h in air to form the composite anode. Then, half-cells with three kinds of different porosities were prepared. Subsequently, Pt paste was painted as a ring around the LSM electrode as the reference electrode (RE) and also painted onto the other side of the YSZ electrolyte disc as the counter electrode (CE). Pt wires were stuck on the composite anode, the RE and the CE, respectively. The Pt electrodes were fired at 850 °C for 20 min in air.

2.2. Characterization

The phase purity of the LSM powders was checked by an X-ray diffractometer (D8 Advance, BRUKER Corporation, Germany). Chemical compatibility of the LSM with the YSZ was investigated by calcination of composite powders at 1000 °C for 20 h. The resulted mixtures were studied by XRD to identify phases. The morphology and pore size of the anodes were observed by a field emission scanning electronic microscope (FESEM, QUANTA 200F, FEI Corporation, USA).

The porosities of the samples were measured by Archimedes method. To ensure water saturation, the samples were immersed in boiling water for 4 h and allowed to cool in water before weighing. Specific surface area was derived from nitrogen adsorption/desorption isotherms obtained at −196 °C (Micromeritics TriStar II 3020 surface area analyzer), samples were degassed overnight at 200 °C.

Electrochemical impedance measurements were performed using a Solartron 1260 frequency response analyzer, coupled to a Solartron 1287 electrochemical interface controlled by ZPlot software (SOLARTRON, AMETEK Co., Ltd). AC perturbation of 5 mV was applied over the frequency range from 0.1 Hz to 1 MHz. The impedance was measured at 700 °C under the atmosphere ranging from 0 to 60 vol% O_2. pO_2 was obtained from the mixture of N_2 and O_2 (both with a purity of 99.999%). Low pO_2 (≈0 Pa) was achieved using pure N_2, assuming a thermodynamic equilibrium between O_2 and N_2. The gas flow rates were fixed at a flow rate of 100 ml min^{-1} using mass flow controllers. The whole system was allowed to stabilize under each condition before the measurement. The typical stabilization time was at least 0.5 h under high pO_2 (0.1×10^5, 0.2×10^5, 0.4×10^5 and 0.6×10^5 Pa) and 5 h under low pO_2 (≈0 Pa). These oxygen partial pressures correspond to 0, 10, 20, 40 and 60 vol% O_2 (relative to the total amount of O_2 and N_2). In light of the small amplitude of the applied voltage and the small sample size relative to the flow rate and the dimension of the experimental apparatus, the gas composition is safely assumed to be unperturbed during the impedance measurements.

The impedance spectra of polarization resistance (R_p) were fitted according to an equivalent circuit consisting of several RQ circuits with the program ZView (SOLARTRON, AMETEK Co., Ltd). The Q is constant phase element (CPE) which is usually a depressed semi-arc in the complex plane of impedance. The impedance of the CPE is as follows:

$$Z_{CPE(\omega)} = [A_0(j\omega)^n]^{-1} \quad (1)$$

where n is varied between 0 and 1 depending on the depression of the arc. ω and j are the frequency and the imaginary unit, respectively. If n equals 1 then the CPE is identical to that of a capacitor. If n equals 0.5, a 45° line is produced on the Complex-Plane graph. When a CPE is placed in parallel to a resistor, a Cole-Element (depressed semi-circle) is produced. Because the thickness of anode is only 20 μm, the Q produces the same spectrum as a Finite Length Warburg. We used Q to simulate the impedance instead of W (Warburg element).

3. Results and discussion

3.1. Powder characterizations

Fig. 1 shows the XRD patterns of LSM powders (a) and LSM/YSZ composite powders (b). Pattern (a) indicates that the LSM powder has a pure perovskite phase, while pattern (b) demonstrates the coexistence of the YSZ and LSM phases. Only a small mount of impurities ($La_2Zr_2O_7$) has been found in pattern (b), which indicates the compatibility of LSM and YSZ was suitable for measurements because the measurements lasted for less than 20 h, especially at 700 °C. Theoretically, high resistance phase has hardly been formed at less than 1000 °C for short time [23].

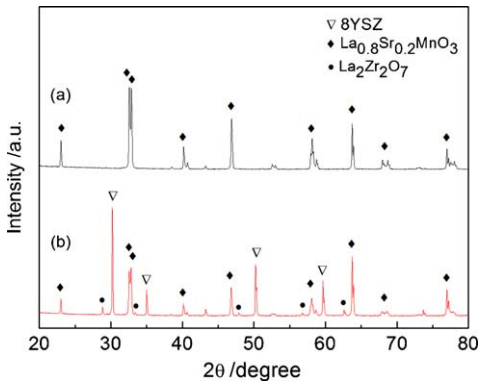

Fig. 1. XRD patterns of sample powders: (a) pure LSM powder, (b) LSM/YSZ composite powder.

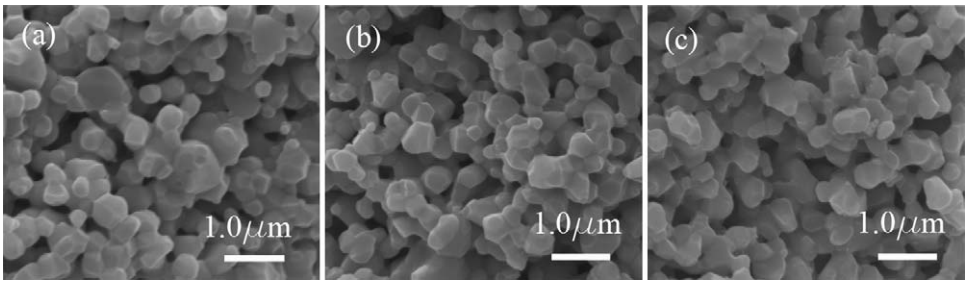

Fig. 2. SEM micrographs of the composite anodes with the porosity of (a) 41 vol%, (b) 46 vol%, and (c) 50 vol%.

3.2. Microstructural analysis

Fig. 2 shows the SEM micrographs of the LSM/YSZ porous composite anodes. It was shown that the grain size is about 500 nm and all the pores are connected. The difference in porosity which was produced by different quantities of pore former (starch) is not large. It is difficult to make a distinction by SEM. As indicated in Fig. 3(a), the porosity of the electrodes increases with the increase of the pore former content. Rational porosity is an important parameter for the TPB of electrode. Larger porosity affects TPB formation. However, conductivity of bulk reduces with the increase of the porosity [24]. Adsorption isotherms calculated from the experimental data are shown in Fig. 3(b). The Langmuir surface area decreases with the increase of the pore former content. This is thought to be due to an increased level of pore former in sample preparation that leads to a higher porosity and, as a consequence, a lower value of final surface area.

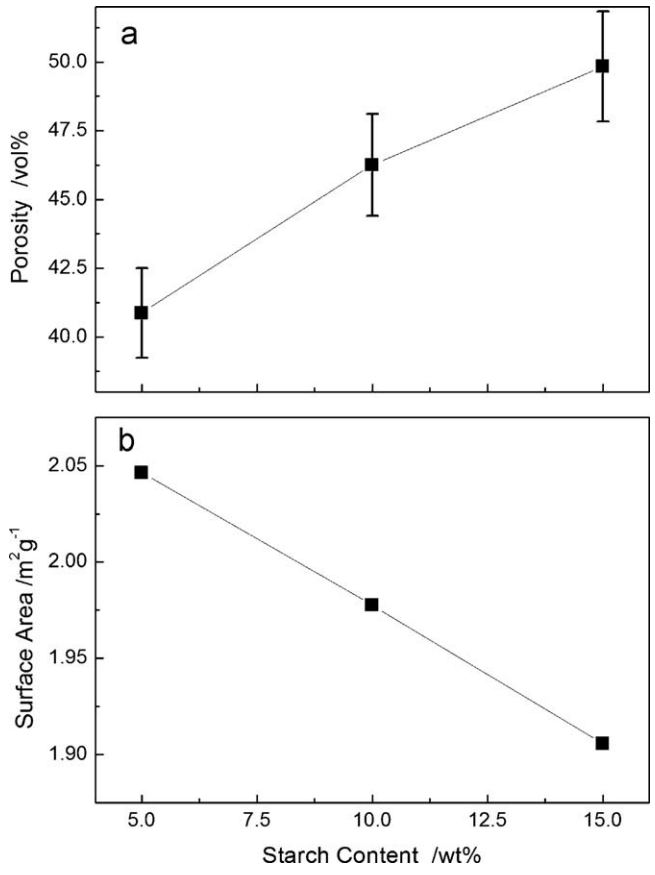

Fig. 3. (a) Relationship between the porosity and the content of pore former, and (b) relationship between the surface area and the content of pore former.

3.3. Electrochemical performance of the half cells

Fig. 4 shows the impedance response of the LSM/YSZ porous electrodes as a function of pO_2 at 700 °C. Fig. 4(a)–(c) is Nyquist diagrams and Fig. 4(d)–(f) is Bode diagrams. Before O_2 feeding to the anode ($pO_2 \approx 0$ Pa) with the porosity of 41 vol%, the initial impedance response of the porous anode was characterized by a large depressed arc and the R_p was 0.7 Ω cm^2. When the pO_2 increased to 0.4×10^5 Pa (40 vol% O_2), the radius of low-frequency arc began to decrease slowly. This phenomenon also appeared in the composite anodes with the porosity of 46 vol% and 50 vol%, as shown in Fig. 4(b) and (c), respectively. However, there is a new separate arc in the impedance spectrum of the sample with the porosity of 50 vol%. It is important to note that all the arcs were dependent on pO_2. The magnitude of the individual arcs was larger for the half cells with high porosity than for those with low porosity, especially when the pO_2 increased from 0 to 0.1×10^5 Pa.

On the other hand, R_p is 1.0 Ω cm^2 for the electrode with the porosity of 46 vol%, which is larger than the other two electrodes. The results showed that the effective conductivity of the porous LSM/YSZ anodes is slightly deviated from that expected on the basis of the average porosity alone. The presence of LSM actually reduces the effective ionic conductivity of the YSZ in the LSM/YSZ composites. While the presence of YSZ reduces the effective electronic conductivity of the LSM in the LSM/YSZ composites [25]. The reduced conductivity is attributed to the increase in the network interruptions and anomalously high constriction resulting from differential densification promoted by the presence of LSM [26]. Conductivity enhancement in the anodes with high porosity is attributed to the more O^{2-} accumulating at the interface of LSM and YSZ. Enhanced carrier (O^{2-}) concentration within the interfacial space charge layers has been proposed as one possible mechanism [27].

At first glance, the spectra in Fig. 4 show two or three separable arcs, especially in Fig. 4(f). The distinction of several arcs is difficult because they are overlapped. In order to obtain more detailed information about the number of the arcs that contribute to the half-cell spectra, the differential analysis of impedance spectra (DIS) was used [28].

The DIS was shown to be helpful in separating electrode arcs originating from different processes in impedance spectra [11,29]. This technique was applied on a half-cell and the produced DIS revealed three separable peaks for the LSM/YSZ electrodes as shown in Fig. 5. The performance of electrochemical cells depends on a sequence of processes, such as charge transfer and non-charge transfer. But the arcs typically overlap in impedance spectra recorded on the half cells. A method is proposed in terms of the change in an impedance spectrum when an optional operation parameter such as pO_2 of a reactant is changed. An impedance spectrum is recorded before such a change and another spectrum recorded just after the change. $\partial \Delta Z'$ is used to selectively detect elements contributing in the impedance spectrum where the

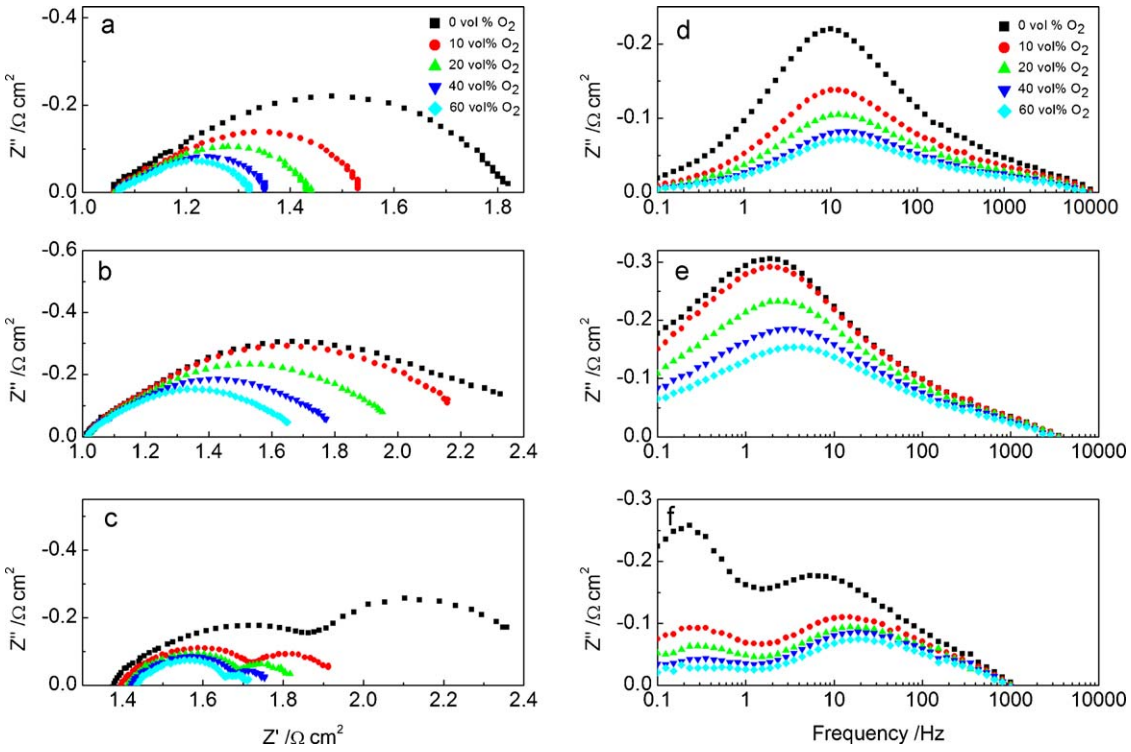

Fig. 4. The change in impedance spectra of the LSM/YSZ composite anodes with different porosities ((a) and (d) 41 vol%, (b) and (e) 46 vol%, (c) and (f) 50 vol%) as a function of pO_2.

contribution may be hidden from other elements. $\partial\Delta Z'$ is listed as the following equation:

$$\partial\Delta Z'(\omega_n) = \frac{[Z'_B(\omega_{n+1}) - Z'_B(\omega_{n-1})] - [Z'_A(\omega_{n+1}) - Z'_A(\omega_{n-1})]}{\ln(\omega_{n+1}) - \ln(\omega_{n-1})} \quad (2)$$

where $Z'_A(\omega)$ is the real part of the impedance in condition A at frequency ω and $Z'_B(\omega)$ is the real part of the other impedance in condition B at frequency ω.

The DIS at open-circuit voltage (OCV) reveals three separable peaks, indicating that at least three processes or reactions at the LSM/YSZ electrode contribute to the impedance spectra in Fig. 5. The characteristic frequency of the anode arcs can be approximated by drawing a straight line through the DIS peaks to the x-axis. Note that the arc for the anode in pure N_2 disappears.

As shown in Fig. 5, investigations on the LSM/YSZ porous electrode in a three-electrode setup revealed three separable arcs with characteristic frequency in good agreement with the low, medium and high frequency peaks, respectively. The arc with characteristic frequency of 500–10,000 Hz was ascribed to O^{2-} transfer from the YSZ to the TPB electrolyte near the YSZ–LSM/YSZ interfaces because the high-frequency arc is not dependent on pO_2. In addition, the arc with characteristic frequency of 10–100 Hz was attributed to

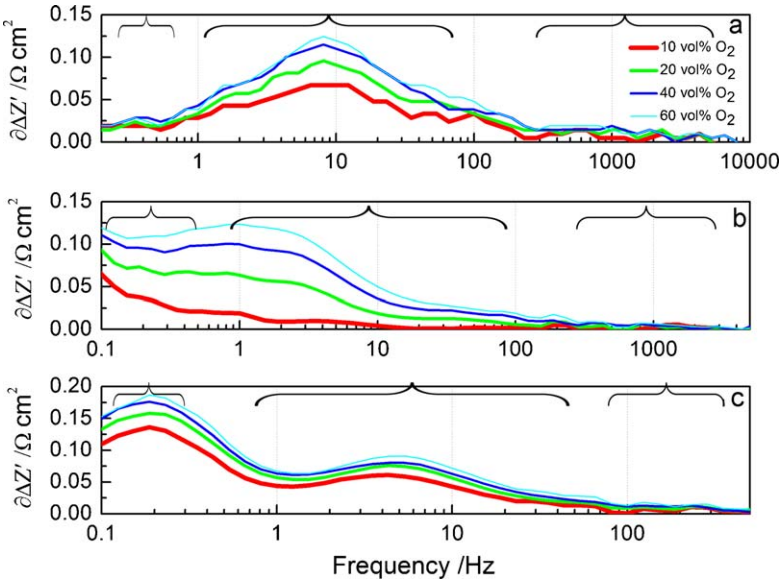

Fig. 5. DIS for the porous LSM/YSZ composite anodes with the porosity of (a) 41 vol%, (b) 46 vol%, and (c) 50 vol% as a function of pO_2.

Fig. 6. Equivalent circuit for the porous LSM/YSZ composite anodes.

dissociative adsorption/desorption of O_2 and transfer of species across the TPB. Moreover, the low frequency arc of 0.1–1 Hz was ascribed to gas diffusion [30,31]. These results were evaluated using the equivalent circuit shown in Fig. 6. The intercepts of the impedance arcs with the real axis at high frequencies corresponded to the resistance of the electrolyte and the lead wires. Here, *R0* was the ohmic resistance of electrolyte and lead wires, and (*R1*, *Q1*), (*R2*, *Q2*) and (*R3*, *Q3*) represent the high-frequency arc, intermediate-frequency arc, and low-frequency arc, respectively. According to previous studies [32], impedance diagrams were composed of several semicircles. Each semicircle or contribution was characterized by the resistance *Ri* (*i* = 1, 2 or 3). In the present study, this means that high, intermediate and low frequency arcs correspond to different electrode processes. The R_p was defined as: $R_p = R1 + R2 + R3$.

3.4. Analysis of discrete circuit element

Fig. 7(a) shows that *R1* increases with increasing pO_2 to a maximum 0.2×10^5 Pa after which the resistance decreases. It is attributed to the carriers obstructed by the increase of pO_2. The high-frequency arc of the LSM/YSZ electrodes did not vary with pO_2 [17]. In the present study, the weak pO_2 dependence of the (*R1*, *Q1*) arc suggests that neither atomic oxygen nor molecular oxygen is involved in the step. Therefore, the (*R1*, *Q1*) arc could be interpreted as O^{2-} transfer from the YSZ electrolyte to the TPB. That is to say, the arc with characteristic frequency about 1 kHz was ascribed to O^{2-} transport at the electrolyte–electrode (YSZ–LSM/YSZ) interface [33]. *R1* is reduced quickly under pO_2 ranging from 0.2×10^5 Pa to 0.6×10^5 Pa for the anodes with the porosity of 46 vol% and 50 vol%. But the impedance of the LSM/YSZ electrode with the porosity of 50 vol% hides the decrease in the transferring resistance of O^{2-}. In fact, the imperfect electrode contacts on solid electrolyte may lead to the increase in resistance (*R1*), which was shown in Fig. 7(a) and (b), and the effect of imperfect electrode contacts cannot be ignored.

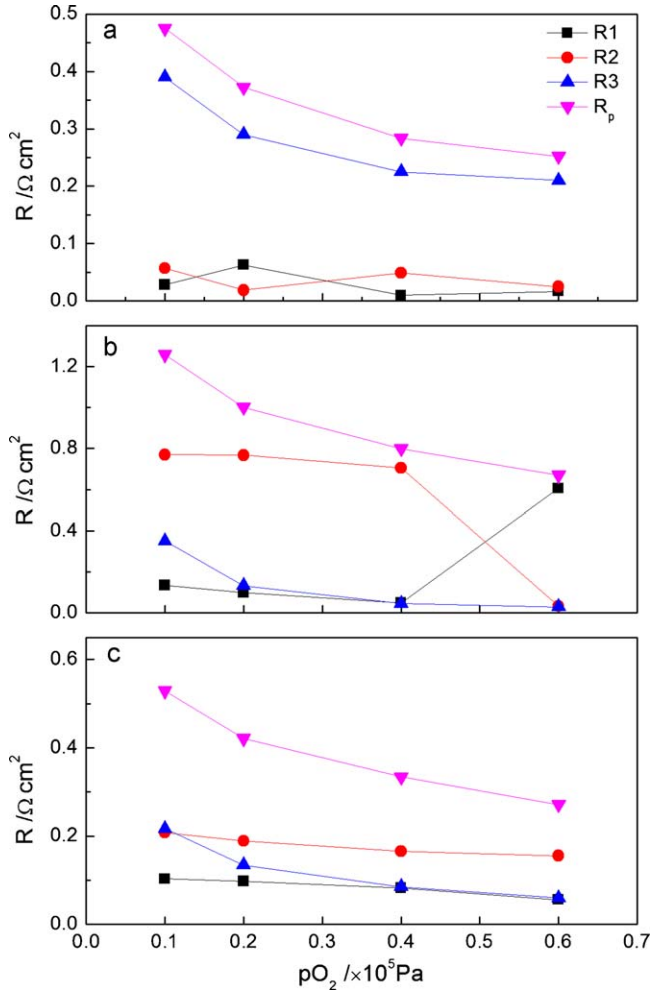

Fig. 7. Polarization resistance of the porous LSM/YSZ composite anodes with the porosity of (a) 41 vol%, (b) 46 vol%, and (c) 50 vol% as a function of pO_2.

As clearly shown in Fig. 4(d)–(f), the characteristics of intermediate-frequency arcs change with pO_2. The processes, such as dissociative desorption of O_2 and transfer of O^{2-} across the TPB, have been proposed to explain the intermediate-frequency arcs [17]. In the present study, the O^{2-} oxidation reaction at the LSM-YSZ interfaces was investigated by modeling the pO_2 dependence. *R2* decreases to a minimum with increasing pO_2 to 0.6×10^5 Pa, which is similar to the variation in O^{2-} transfer. This indicates that O^{2-} surface diffusion is sensitive to pO_2. Finally, the decrease in the *R2* for the electrodes with high porosity is not obvious, which is perhaps due to a greater specific area that facilitates the diffusion process. But there is an abrupt decrease of the *R2* in Fig. 7(b), the arc attributable to O^{2-} surface diffusion weakens under a certain pO_2. It is thought that oxygen vacancies created on the LSM surface enhance O^{2-} surface diffusion. The *R2* increased because the oxygen vacancies are removed by the oxygen exchange reaction between the oxygen molecules and the LSM surface.

It is clear that the low-frequency arc changes significantly with pO_2 as shown in Figs. 4 and 7. The arc below 10 Hz has been ascribed to diffusion losses [31]. It was observed that the variation of the low-frequency arc is comparatively small in the range of measuring pO_2. According to equation [5]:

$$\sigma = en_0 \left(\frac{p_0}{pO_2}\right)^{1/X} \mu_0 \exp\left(\frac{-E_A}{kT}\right) \quad (3)$$

where *X* is the reciprocal potential factor in the dependence of σ on pO_2. p_0 is a pressure for normalization. n_0 and μ_0 are exponential pre-factors if *n* and μ depend exponentially on *T*. The exponential dependence of *n* is given by the ionization energy of the donor states (E_i) and by the enthalpy of reduction ($\Delta H = YE_A$ if E_A is completely determined by the reduction reaction, *Y* is a number which is given by the reaction). The weak variation of *R3* with pO_2 indicates the activation energy of (*R3*, *Q3*) arc is therefore low. This reaction could be interpreted as the diffusion of oxygen molecules in electrode pores or the associative desorption of O_2.

As shown in Fig. 8, the specific conductivity (R_p^{-1}) of the porous LSM/YSZ anodes has been investigated as a function of pO_2. The R_p^{-1} is approximately proportional to $(pO_2)^{0.36}$. The value of 0.36 is different from previous study of dense LSM/YSZ composite (0.25) [15], which indicates the specific conductivity is effected by the porosity. Although $(pO_2)^{0.36}$ dependence is generally interpreted as a charge transfer reaction, these results indicate that $(pO_2)^{0.36}$ dependence could be O^{2-} motion. Therefore, it is con-

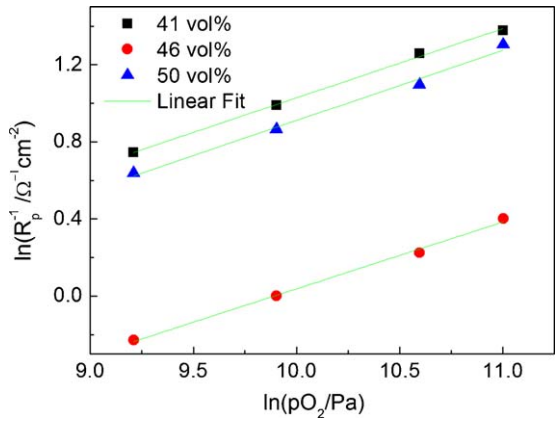

Fig. 8. Dependence of the specific conductivity on pO_2 for the LSM/YSZ anodes with different porosities.

cluded that high-frequency arcs (*R1*, *Q1*) represent O^{2-} transfer from the electrolyte to the TPB, and intermediate-frequency arcs (*R2*, *Q2*) represent the diffusion of O^{2-} species along the LSM surface to the TPB.

4. Conclusions

The electrochemical behavior of the LSM/YSZ porous composite anodes was investigated by EIS under different pO_2. In particular, DIS revealed three identifiable peaks of charge transfer and non-charge transfer at the LSM/YSZ electrodes. The high-frequency arc was attributed to oxygen ion transfer from the electrolyte to the TPB, which is independent on pO_2. In addition, the intermediate-frequency arc was ascribed to dissociative desorption of O^{2-} along the LSM surface, which is dependent on pO_2. Moreover, the low-frequency arc was attributed to gas phase diffusion, which is also dependent on pO_2. With the increase of porosity, the positions of the peaks in DIS moved to lower frequency, and the arcs in EIS become clearly separated at different frequencies.

Acknowledgment

This work was supported by the Chinese major project of national science and technology (2010ZX06901-020). Funding from Tsinghua University (Contract Number: 20101081790) and State Key Lab of New Ceramics and Fine processing of Tsinghua University were also gratefully acknowledged (2010THZ08).

References

[1] P. Kim-Lohsoontorn, D.J.L. Brett, N. Laosiripojana, Y.M. Kim, J.M. Bae, Int. J. Hydrogen Energy 35 (2010) 3958–3966.
[2] M.A. Laguna-Bercero, J.A. Kilner, S.J. Skinner, Chem. Mater. 22 (2010) 1134–1141.
[3] S.P. Jiang, J.G. Love, J.P. Zhang, M. Hoang, Y. Ramprakash, A.E. Hughes, S.P.S. Badwal, Solid State Ionics 121 (1999) 1–10.
[4] T. Dittrich, E.A. Lebedev, J. Weidmann, Phys. Status Solidi A 165 (1998) R5–R6.
[5] T. Dittrich, J. Weidmann, F. Koch, I. Uhlendorf, I. Lauermann, Appl. Phys. Lett. 75 (1999) 3980–3982.
[6] E.A. Lebedev, E.A. Smorgonskaya, G. Polisski, Phys. Rev. B 57 (1998) 14607–14610.
[7] M. Mogensen, S. Skaarup, Solid State Ionics 86 (1996) 1151–1160.
[8] J. Newman, W. Tiedemann, Molecules 24 (1956) 25–41.
[9] J. Kong, Y. Zhang, C. Deng, J. Xu, J. Power Sources 186 (2009) 485–489.
[10] M. Liang, B. Yu, M. Wen, J. Chen, J. Xu, Y. Zhai, J. Power Sources 190 (2009) 341–345.
[11] A. Hauch, S.H. Jensen, S. Ramousse, M. Mogensen, J. Electrochem. Soc. 153 (2006) A1741–A1747.
[12] A. Brisse, J. Schefold, M. Zahid, Int. J. Hydrogen Energy 33 (2008) 5375–5382.
[13] E. Siebert, A. Hammouche, M. Kleitz, Electrochim. Acta 40 (1995) 1741–1753.
[14] J. Mizusaki, N. Mori, H. Takai, Y. Yonemura, H. Minamiue, H. Tagawa, M. Dokiya, H. Inaba, K. Naraya, T. Sasamoto, T. Hashimoto, Solid State Ionics 129 (2000) 163–177.
[15] J.D. Kim, G.D. Kim, J.W. Moon, Y. Park, W.H. Lee, K. Kobayashi, M. Nagai, C.E. Kim, Solid State Ionics 143 (2001) 379–389.
[16] J. Van Herle, A.J. McEvoy, K.R. Thampi, Electrochim. Acta 41 (1996) 1447–1454.
[17] S.P. Jiang, J.G. Love, Y. Ramprakash, J. Power Sources 110 (2002) 201–208.
[18] X.J. Chen, K.A. Khor, S.H. Chan, Solid State Ionics 167 (2004) 379–387.
[19] S.P. Jiang, J.P. Zhang, K. Foger, J. Electrochem. Soc. 147 (2000) 3195–3205.
[20] T. Horita, K. Yamaji, M. Ishikawa, N. Sakai, H. Yokokawa, T. Kawada, T. Kato, J. Electrochem. Soc. 145 (1998) 3196–3202.
[21] H. Kamata, A. Hosaka, J. Mizusaki, H. Tagawa, Solid State Ionics 106 (1998) 237–245.
[22] F.H. Van Heuveln, H.J.M. Bouwmeester, F.P.F. van Berkel, J. Electrochem. Soc. 144 (1997) 126–133.
[23] M. Chen, Y.L. Liu, A. Hagen, P.V. Hendriksen, F.W. Poulsen, Fuel Cells 9 (2009) 833–840.
[24] S.B. Adler, Chem. Rev. 104 (2004) 4791–4844.
[25] Y. Ji, J.A. Kilner, M.F. Carolan, Solid State Ionics 176 (2005) 937–943.
[26] K. Yamahara, T.Z. Sholklapper, C.P. Jacobson, S.J. Visco, L.C. De Jonghe, Solid State Ionics 176 (2005) 1359–1364.
[27] S. Lanfredi, L. Dessemond, A. Rodrigues, J. Am. Ceram. Soc. 86 (2003) 291–298.
[28] S.H. Jensen, A. Hauch, P.V. Hendriksen, M. Mogensen, N. Bonanos, T. Jacobsen, J. Electrochem. Soc. 154 (2007) B1325–B1330.
[29] S.H. Jensen, A. Hauch, P.V. Hendriksen, M. Mogensen, J. Electrochem. Soc. 156 (2009) B757–B764.
[30] M.J. Jørgensen, M. Mogensen, J. Electrochem. Soc. 148 (2001) 433–442.
[31] R. Barfod, A. Hagen, S. Ramousse, P.V. Hendriksen, M. Mogensen, Fuel Cells 6 (2006) 141–145.
[32] M. Guillodo, P. Vernoux, J. Fouletier, Solid State Ionics 127 (2000) 99–107.
[33] B. Kenney, K. Karan, J. Electrochem. Soc. 157 (2010) B1126–B1137.